Tropical upper tropospheric clouds: variation with sea surface temperature and radiative effects

Hui Su, Jonathan H. Jiang, Yu Gu[1], J. David Neelin[1], Brian H. Kahn, Daniel Feldman[2], Yuk L. Yung[2], Joe W. Waters, Nathaniel J. Livesey, Michelle L. Santee

Jet Propulsion Laboratory, California Institute of Technology, Pasadena, California, 91109, USA

[1]Department of Atmospheric and Oceanic Sciences, University of California, Los Angeles, CA 90095, USA.

[2]Division of Geological and Planetary Sciences, California Institute of Technology, Pasadena, CA, 91125, USA

Hui Su, M/S 183-701, Jet Propulsion Laboratory, California Institute of Technology, 4800 Oak Grove Drive, Pasadena, California 91109-8099, U.S.A.

(Email: Hui.Su@jpl.nasa.gov)

Abstract. The variations of tropical upper tropospheric clouds (UTC) with sea surface temperature (SST) are analyzed in terms of cloud fraction (CFR) from the Atmospheric Infrared Sounder (AIRS) on Aqua and ice water content (IWC) from the Microwave Limb Sounder (MLS) on Aura. The SST data are from the Advanced Microwave Scanning Radiometer (AMSR-E) on Aqua. It is found that the daily mean CFR over tropical cloudy areas is nearly invariant with the mean under-cloud SST, while the daily mean IWC and ice water path (IWP, integrated IWC above 215 hPa) over tropical cloudy areas increase with the mean under-cloud SST at a rate about 20% per degree K, faster than the increase of daily mean cloudy-area precipitation with SST. The net radiative effect of the observed UTC is to warm the Earth-atmosphere system. The amplitude of the net warming is about 7-17 W m^{-2} in the tropical average, with uncertainty largely arising from the estimate of fractional coverage of UTC. The net UTC radiative effect (CRE) varies approximately monotonically with CFR, but non-monotonically with IWP. The increase of IWP with SST would yield an increase of net warming of about 0.1 W m^{-2} K^{-1}, corresponding to a positive feedback, until the net warming reaches a maximum when IWP is increased by 50%. Doubling of IWP yields almost no change in the net CRE, although the changes in LW and SW CRE individually are substantial, about 3.2 W m^{-2} averaged over the tropics.

1. Introduction

High-altitude clouds have important radiative effects on the Earth-atmosphere system. They are closely related to upper tropospheric humidity (UTH), which contributes dominantly to the greenhouse effect [e.g. Betts 1990; Lindzen 1990; Sun and Lindzen 1993; Udelhofen and Hartmann 1995; Soden and Fu 1995; Su et al. 2006]. They also provide significant radiative forcing to the climate system. Their net radiative effect results from a balance between warming by reducing terrestrial emission to space and cooling by reflecting incoming solar radiation. Quantification of the net effect is subject to errors in both longwave (LW) and shortwave (SW) radiative flux measurements, and in model calculations. The net cloud radiative effect (CRE) of high-level clouds depends on cloud height, optical thickness, areal fraction and cloud microphysical properties such as ice particle size and ice habits. Accurate representation of clouds and their radiative effects and associated climate feedbacks is one of the greatest challenges in climate model simulations and climate change predictions (Cess et al. 1990, 1996; Stephens 2005).

High-altitude clouds in the tropics include deep convective towers and associated anvil clouds, as well as thin cirrus that can be formed in situ by gravity wave and Kelvin wave perturbations or by large-scale uplift of humid layers (Massie et al. 2002). The relationships of deep convective clouds and anvils clouds to SST are of great interest in climate studies because of their importance for cumulus parameterizations in models and their potential implications for cloud feedbacks in climate change. A number of studies have been conducted using various measures of cloud observations and numerical models (e.g. Graham and Barnett 1987; Waliser et al. 1993; Ramanathan and Collins 1991, hereafter RC1991; Lau et al. 1997; Tompkins and Craig 1999; Lindzen et al. 2001, hereafter LCH2001; Hartmann and Larson 2002; Del Genio and Kovari 2002;

Bony et al. 2004; Lin et al. 2006). However, no consensus has been reached regarding whether high-altitude clouds increase or decrease with SST and whether they provide a positive or negative climate feedback. For example, RC1991 showed that the radiative forcing of cirrus anvils increases during El Niño events; and the increase of their SW cooling effect is larger than the increase of their LW warming effect. This suggests that the optical thickness of cirrus anvils may increase when SST increases, in addition to the increase in the extent of cloudiness and the height of cloud top. They speculated that cirrus anvils may act like a "thermostat" to limit further warming of SST. This viewpoint has been challenged by a number of studies that highlighted the roles of evaporation, large-scale circulation, and ocean dynamics in regulating tropical SST (Wallace 1992; Fu et al. 1992; Hartmann and Michelsen 1993; Pierrehumbert 1995; Sun and Liu 1996).

Another viewpoint regarding the cirrus-SST relation and its climate feedback is the "iris hypothesis" proposed in LCH2001, in which the cirrus fractional coverage variation with SST was analyzed based on the infrared brightness temperature (11 and 12 μm channels) from the Japanese Geostationary Meteorological Satellite (GMS). LCH2001 showed that cirrus coverage normalized by cumulus coverage decreases about 22% per degree increase of SST, analogous to an eye's iris when exposed to stronger light. They further inferred that the "iris" effect would produce a strong negative climate feedback. There has been intense debate about the validity of the "iris hypothesis" in terms of the analysis approach and interpretation of the results (Hartmann and Michelsen 2002; Lindzen et al. 2002) as well as the assumptions about the radiative properties of high clouds (Fu et al. 2002; Lin et al. 2002; Chambers et al. 2002; Chou et al. 2002, 2002b). Del Genio and Kovari (2002) analyzed the Tropical Rainfall Measuring Mission (TRMM) data and found that precipitation efficiency and cirrus detrainment efficiency both increase with increasing

SST, with the former increasing faster than the latter. However, the TRMM cloud data are biased towards precipitating deep convective clouds, and a different relation may apply to cirrus anvil clouds alone. Lack of direct observations of the amount of deep convective cores and cirrus anvils hinders resolution of the “iris” debate.

New satellite observations from the National Aeronautics and Space Administration (NASA)’s “A-train” satellite constellation (Schoeberl and Talabac 2006) provide new information on global cloud variability. The A-train satellites are sun-synchronous, with an equatorial crossing time around 1:30 am and 1:30 pm. The orbit tracks repeat every 16 days. In particular, the Atmospheric Infrared Sounder (AIRS) on the Aqua satellite (Parkinson 2003; Chahine et al. 2006) provides cloud fraction (CFR) and cloud top pressure (CTP), starting from September 2002. The Microwave Limb Sounder (MLS) on the Aura satellite (Schoeberl et al. 2006; Waters et al. 2006), for the first time, provides the upper tropospheric (UT) ice water content (IWC) profile at 215 hPa and above, starting from August 2004. The ice water path (IWP) can then be computed by the mass-weighted vertical integration of IWC from 215 hPa to the cloud top heights. The AIRS and MLS observations are only about 8 minutes apart (Kahn et al. 2007), and there are about 5-6 AIRS measurements within each MLS field of view (FOV). CloudSat and Calipso are new members of the A-train that started to produce cloud liquid and ice water content profiles throughout the troposphere in June 2006 (Stephens et al. 2002). Because the CloudSat/Calipso data temporal coverage is too short for this study, we defer analysis of these data for future work.

In this study, we examine variations of the UT cloud fraction from AIRS and the UT IWC/IWP from MLS in relation to the underlying SST, obtained from the microwave SST analysis from the Advanced Microwave Scanning Radiometer (AMSR-E) on Aqua. We use upper tropospheric clouds (UTC) to refer to the high-altitude clouds observed by AIRS and MLS without distinction between different cloud types. Separation of deep convective cores, anvil clouds and thin cirrus will be explored in future work. In contrast to a recent study by Su et al. (2006), which analyzed the spatial correlation of MLS IWC/IWP with SST on monthly and annual time scales, this paper focuses on the temporal variation of CFR and IWC/IWP of the UTC on a daily time scale, as in LCH. We examine the relationship between the daily CFR and IWC/IWP averaged over all tropical cloudy areas and the daily mean under-cloud SST (see section 3 for details). The surface precipitation variation with SST is also analyzed using precipitation data from TRMM. One of the issues in analyzing the clouds and SST relation is how to account for the impact of changing large-scale circulation associated with SST gradients on clouds (Lindzen and Nigam 1987; Hartmann and Michelsen 1993; Lau et al. 1997; Bony et al. 2004). LCH2001 postulated a normalization procedure in which cirrus anvil coverage was divided by the cumulus coverage. It attempts to deal with the varying detrainment from cumulus convection when SST changes rather than varying cumulus convection itself with SST, which may be related to shifting patterns of large-scale circulation and SST gradients. Such an attempt is reasonable and the normalization would work only if cirrus anvil coverage were proportional to the cumulus coverage. Here, we experiment with an analogous procedure to that used in LCH2001: we use precipitation to normalize CFR or IWP by dividing the cloudy-area mean CFR or IWP by the cloudy-area mean precipitation. The relationships of the precipitation-normalized CFR and IWP with the mean under-cloud SST are analyzed and the intricacy of the normalization procedure is also addressed. The UTC-SST relationships from our observational data analysis will serve as useful reference values for cloud simulations in climate models. It also helps to shed light on the inference of UT cloud changes for future climate.

A radiative transfer model is employed to estimate the radiative effect of the observed UTC. Both the monthly-mean and the daily distribution of UTC radiative effect as a function of CFR and IWP are presented. They provide useful insights on cloud radiation feedback.

The structure of the paper is as follows. Section 2 describes the datasets used for the analyses. Section 3 presents the UTC and SST relations based on the AIRS and MLS observations. The radiative effect of the UTC is discussed in Section 4. Conclusion and discussion are given in Section 5.

2. Data

The AIRS Level 3 cloud fraction (CFR) data are provided on 1°×1° horizontal grids and are available daily from September 1, 2002 to September 30, 2006 (version 4, Olsen et al. 2005). The AIRS CFR retrieval uses a radiance fitting procedure described in Susskind et al. (2003), with a horizontal resolution of ~15 km. To identify high-altitude clouds, we use the simultaneous AIRS Level 3 cloud top pressure (CTP) measurements. Only grid boxes with CTP < 300 hPa are considered UTC. This value is chosen to match the MLS IWC measurement, which only goes down to 215 hPa. The AIRS CTP measurement has a horizontal FOV of ~ 45 km in diameter (Kahn et al. 2007). Early cross-comparison between the AIRS and MLS cloud measurements found that AIRS CTP tends to have a high (in pressure levels) bias compared to that derived from the MLS IWC measurements (Kahn et al. 2007; Wu et al. 2007). We find that the results are not sensitive to the exact choices of CTP values between 450-200 hPa. Throughout the rest of the discussions, we use CFR to denote the UTC fraction with CTP < 300 hPa. Note that the AIRS CFR represents a combined effect of cloud areal coverage and cloud emissivity. For thick clouds, the emissivity is close to 1. Hence, their CFR is approximately fractional coverage. However, for thin clouds that are not opaque, the retrieved CFR is smaller than the actual cloud coverage.

Preliminary analysis indicates that the difference between the AIRS retrieved CFR and the actual cloud coverage is about 0.2 in the global average (B. Kahn, personal communication, 2007). Such caveats need to be considered when interpreting the analysis results.

The Aura MLS Level 2 IWC measurement is available from August 8, 2004 to September 30, 2006 (version 1.5). The IWC is retrieved from the cloud-induced radiance at 240 GHz (Wu et al. 2006). The v1.5 IWC is available at 215, 178, 147, 121, 100, 83 and 68 hPa, with a horizontal resolution of 200-300 km along-track and ~7 km cross-track, and a vertical resolution of 3-4 km (Livesey et al. 2005; Wu et al. 2006, 2007). The Aura MLS IWC data have been validated against in situ aircraft measurements and other satellite data (Wu et al. 2007), and have been compared with model simulations and analyses (Li et al. 2005). The estimated IWC absolute accuracy is within a factor of 2 and there may be a low bias around 50% compared to CloudSat IWC (Wu et al. 2007). The spatial pattern of the MLS IWC resembles deep convective systems and associated anvil clouds (Li et al. 2005, Su et al. 2006). The Level 2 data are obtained along MLS orbit tracks. The gap between orbits is about 25° in the tropics (30ºS-30ºN). The number of profiles each day is about 3500, with one-third of them within the tropics.

We use the daily microwave SST product from the AMSR-E on the Aqua satellite (version 2, Donlon et al 2002), processed at Remote Sensing Systems with a horizontal resolution of 0.25°×0.25°. To reduce sampling errors, we average the AMSR-E SST to both AIRS and MLS data grids when performing correlation analyses. The through-cloud capabilities of microwave radiometers reduce the influence of clouds on the SST retrieval, and the daily coverage of the AMSR-E SST is a significant improvement from the weekly SST product from the National Centers for Environmental Prediction (NCEP) analysis, which was used in LCH.

We use the daily TRMM precipitation data (3B42, Huffman et al. 2001) at a horizontal resolution of 0.25°×0.25°. Averaging onto the AIRS and MLS data grids is performed for coincident sampling, as for the AMSR-E SST.

3. UTC-SST Relations

We define a daily mean UTC amount as $\overline{A}^c = \sum_n \cos\theta \cdot A_n \Big/ \sum_n \cos\theta$, where A is either CFR, IWC or IWP, θ is the latitude within 30°S-30°N, and n includes only tropical oceanic "cloudy" measurements defined by the CFR greater than zero in a 1º×1º grid box or the individual measurements of IWC in the MLS FOV above the 3-σ MLS cloud detection threshold (Livesey et al. 2005). An analogous definition is used for the mean under-cloud SST. These definitions do not include clear-region quantities and focus on the local relations of UTC and SST for the entire cloudy regions. They represent the cloudy tropics as one box with varying boundary based on the daily UTC measurements. We regard SST as a forcing to the convective systems on a daily time scale. The fraction of the measurements that are cloudy is about 15-20% for AIRS CFR and 6-10% for MLS IWC, and both of which stay approximately constant with changes in the mean under-cloud SST. Thus the cloudy-area mean CFR or IWC/IWP scale approximately linearly with the tropical-mean CFR or IWC/IWP, which include the clear-sky regions.

Insert Figure 1 here

a. AIRS CFR-SST Relation

Figure 1a shows the AIRS mean cloudy-area UTC fraction ($\overline{CFR}^c$) scattered against the mean under-cloud SST for the period of September 1, 2002 to September 30, 2006. Each dot corresponds to a daily average. All daily $\overline{CFR}^c$ occurs over the mean under-cloud SST greater than

300 K, indicating the close connection of AIRS observed UTC to tropical deep convection (e.g. Graham and Barnett 1987; Waliser et al. 1993; Su et al. 2006). The daily $\overline{CFR}^{c}$ is very scattered with respect to the mean under-cloud SST, with a correlation coefficient of 0.054 and a linear regression slope of 0.52 % K^{-1} (~2% K^{-1} relative to the 4-year mean CFR). The Student's t-test finds that this correlation coefficient barely rejects the null hypothesis that the true correlation coefficient is zero. If we restrict the area to 20ºS-20ºN or 10ºS-10ºN, the regression slopes are 1.2% K^{-1} and 2.6% K^{-1}, corresponding to 4% K^{-1} and 8% K^{-1} relative to the 4-year means, respectively (Table 1). The smaller regression slopes of the $\overline{CFR}^{c}$ versus the mean under-cloud SST when more subtropical regions are included in the averaging may imply the influence of subtropical meteorological forcing on convection and cirrus outflow (Hartmann and Michelsen 2002). If we restrict the averaging area to the western Pacific from 130ºE to 170ºW (30ºS-30ºN) as in LCH2001, the slope of CFR versus SST is 2.2% K^{-1}, or 6% K^{-1} relative to its 4-year mean (Table 1). Given the small correlation between the $\overline{CFR}^{c}$ and the mean under-cloud SST, it is fair to say that the $\overline{CFR}^{c}$ is nearly invariant with the mean under-cloud SST.

Figure 1b shows the scatter plot of the $\overline{CFR}^{c}$ versus the cloud-area mean precipitation ($\overline{P}^{c}$). The correlation coefficient between $\overline{CFR}^{c}$ and $\overline{P}^{c}$ is 0.68, statistically significant above the 95% level. When the $\overline{P}^{c}$ is scattered against the mean under-cloud SST, a positive correlation of 0.31 is found (Fig. 1c). The $\overline{P}^{c}$ increases with the mean under-cloud SST at a rate of 0.34 mm day^{-1} K^{-1}, about 22% K^{-1}, relative to its 4-year mean. The increase of precipitation with local SST is not surprising, and an increase of UTC fraction with precipitation is expected since the deep convection that produces the precipitation also contributes to the clouds. However, there are a number of aspects to these relationships that are far from simple. The most obvious is that despite the relationship of cloud fraction to precipitation (Fig. 1b), and of precipitation to SST (Fig. 1c), the relationship of cloud fraction to SST is highly scattered. We note that combining the regression coefficients of Figs. 1b and 1c leads to CFR′ = 2.8 SST′, where primes denotes departure from the mean, a slope much larger than is seen in Fig. 1a. Given the explained variance of cloud fraction by precipitation is about 50% and the explained variance of precipitation by SST is about 10%, a large portion of the cloud fraction variation is not explained by SST changes. Part of the AIRS observed UTC could be formed in situ and consequently may not exhibit a simple relation with the underlying SST. Even for the cirrus clouds that are of convective origin, factors other than SST may play important roles in the cirrus outflow, such as UT temperature (Chou and Neelin 1999) and aerosol concentration (Liu et al. 2007).

We also note that the cloud fraction dependence on precipitation has a considerably lower slope than if cloud fraction were simply proportional to precipitation. For reference, the regression line constrained to go through zero is shown in Fig. 1b (the dotted line). The non-proportionality between $\overline{CFR}^c$ and $\overline{P}^c$ has considerable consequence if one wishes to use precipitation to normalize cloud fraction, in a procedure analogous to LCH2001 normalization by a measure of cumulus area. If cloud fraction were proportional to precipitation then dividing by precipitation would remove the precipitation dependence. As it is (Fig. 1b), dividing cloud fraction by precipitation would result in a term inversely proportional to the mean precipitation in addition to the regression slope of cloud fraction to precipitation, and only the latter is the quantity of relevance to the detrainment of cirrus clouds per unit convection. Figure 1d shows what happens if one takes the ratio of cloud fraction to precipitation for each day and scatters the ratio against the mean under-cloud SST. The precipitation-normalized cloud fraction appears to decrease with increasing SST at a rate of –5% mm^{-1} day K^{-1} (Fig. 1d), corresponding to –24% K^{-1} relative to the 4-year mean. The rate of decrease of the precipitation-normalized CFR with SST is close to the rate of decrease of the cumulus-normalized cirrus coverage with SST in LCH2001. The correlation coefficient between the precipitation-normalized CFR and the mean under-cloud SST is –0.4, statistically significant above the 95% level. For tropical bands between 20ºS-20ºN and 10ºS-10ºN, the precipitation-normalized CFR also decreases with SST by about –20% K^{-1} (Table 1). For the region analyzed in LCH2001, the slope of the normalized AIRS CFR versus SST is about –12% K^{-1} with a correlation coefficient around –0.2. Considering that the AIRS CFR depends upon both emissivity and areal coverage, the actual cirrus areal coverage may be higher than the CFR, especially for thin cirrus. This would increase the negative slope in Fig. 1d if warmer SST is associated with thicker UTC.

The decrease of the precipitation-normalized CFR with SST is expected, given the nearly invariant $\overline{CFR}^c$ with SST in Fig. 1a and the increase of $\overline{P}^c$ with SST in Fig. 1c. The rate of decrease of $\overline{CFR}^c / \overline{P}^c$ with SST is dominated by the term inversely proportional to precipitation, which would produce a decreasing tendency with SST at around –20% K^{-1}. Hence, although the normalization is appealing, simply dividing the cloud fraction by precipitation does not provide a good solution to isolate the cirrus detrainment change from the cumulus convection change itself. Based on the relations shown in Fig. 1, we conclude that UTC fraction does not vary significantly with the mean under-cloud SST, while precipitation increases noticeably with increasing SST. Given the non-proportionality between cloud fraction and precipitation, we are inclined to be cautious about inferring cirrus detrainment change using this normalization procedure.

On the other hand, CFR is only one measure of UTC amount. Cloud optical depth, which is dependent on IWC and cloud height, is another important property that affects the radiative effect of the clouds. It is possible that IWC and cloud height could undergo significant changes when the surface warms, which in turn could alter the net radiative forcing of the UTC in addition to the changes caused by the CFR variations. Hence, we analyze the IWC and cloud height information from MLS to better quantify the UTC variation with SST and the associated radiative impact.

Insert Figure 2 here

b. MLS IWC-SST Relation

Figure 2 shows the daily MLS IWC scattered against the mean under-cloud SST during the period from August 8, 2004 to September 30, 2006. For each day, the mean under-cloud SST is computed using the AMSR-E SST averaged into the areas centered on the MLS measurement location and spanning ±1° along track and ±0.5° cross track. Three vertical levels of IWC are displayed in Figure 2, 100 hPa (~16 km), 147 hPa (~13.5 km) and 215 hPa (~11 km). All show an increase of $\overline{IWC}^c$ with increasing mean under-cloud SST, albeit with a large scatter. The rates of the $\overline{IWC}^c$ increase with the mean under-cloud SST are 1.6 mg m^{-3} K^{-1} at 215 hPa, 1.2 mg m^{-3} K^{-1} at 147 hPa and 0.2 mg m^{-3} K^{-1} at 100 hPa. The percentage changes relative to the 2-year mean at each level are approximately 9% K^{-1} at 215 hPa, 22% K^{-1} at 147 hPa, and 13% K^{-1} at 100 hPa. The correlation coefficients between the $\overline{IWC}^c$ and the mean under-cloud SST are 0.42 at 215 hPa, 0.49 at 147 hPa and 0.28 at 100 hPa, all statistically significant above the 95% level. Similar analysis is performed for 10ºS-10ºN and 20ºS-20ºN bands, where the increase of $\overline{IWC}^c$ with the mean under-cloud SST occurs at a slightly higher rate (not shown).

We also define a MLS CTP as the minimum pressure level at which the MLS IWC is above the 3σ detection threshold. Fig. 2d shows the mean MLS CTP over the cloudy-areas ($\overline{CTP}^c$) versus the mean under-cloud SST. It shows that MLS $\overline{CTP}^c$ increases in height (decreases in pressure) when SST increases, at roughly –5 hPa K^{-1}.

Insert Figure 3 here

With the increasing cloud height and increasing IWC at each level, the vertically-integrated IWP (from 215 hPa and up) increases with SST, as displayed in Fig. 3a. The rate of the increase of the $\overline{IWP}^c$ with the mean under-cloud SST is 5.3 g m^{-2} K^{-1}, about 20% K^{-1} relative to the 2-year mean IWP. The correlation between the $\overline{IWP}^c$ and the mean under-cloud SST is about 0.5. The mean precipitation over the MLS observed cloudy areas (where the MLS IWP is above the cloud detection threshold), $\overline{P}^c$, is constructed and its relation to $\overline{IWP}^c$ and the mean under-cloud SST are displayed in Fig. 3b and 3c, respectively. Note that the $\overline{P}^c$ based on the MLS IWP is generally higher than the $\overline{P}^c$ based on the AIRS CFR (cf. Fig. 1c). This indicates that the MLS-detected UTC is more closely tied to precipitating convective systems than the AIRS-detected UTC. Infrared instruments such as AIRS may detect more thin cirrus away from precipitating cumulus towers than microwave instruments such as MLS. It is shown that $\overline{P}^c$ increases with the mean under-cloud SST at the rate of 0.43 mm day^{-1} K^{-1}, about 12% K^{-1} relative to the 2-year mean. It is positively correlated with $\overline{IWP}^c$ with a correlation coefficient of 0.5. However, we note that $\overline{IWP}^c$ and $\overline{P}^c$ are not proportional, indicated by the two different slopes for the least-squares fitted line and the line constrained to go through zero. Thus the relation of the precipitation-normalized IWP with SST (Fig. 3d) does not remove the precipitation dependence on SST, similar to the precipitation-normalized CFR shown in Fig. 1d. Despite that the term inversely proportionally to precipitation would yield a negative tendency for the precipitation-normalized IWP relation with SST, the normalized IWP exhibits a positive slope with the mean under-cloud SST, at the rate about 8% K^{-1}, with a correlation coefficient of 0.15. Similar results are found for other tropical bands and the region used in LCH2001. It is robust that $\overline{IWP}^c$ increases with increasing SST, at a rate faster than the increase of $\overline{P}^c$ with the mean under-cloud SST. These results are useful for evaluation of model simulations in the current climate.

So far, we find that cloud fraction appears not sensitive to SST changes but the IWC (IWP) has a clear increasing tendency with SST. Therefore, we employ a radiative transfer model to examine the radiative effect of the UTC and how the radiative effect varies when IWC changes.

4. The UTC radiative effect

The radiative transfer model we use is the Fu-Liou radiation model. It uses the delta-four-stream approximation for solar flux calculations (Liou et al. 1988) and delta-two-stream approximation for infrared flux calculations (Fu et al. 1997). The incorporation of non-grey gaseous absorption in multiple-scattering atmospheres is based on the correlated *k*-distribution method developed by Fu and Liou (1992). The solar and infrared spectra are divided into 6 and 12 bands, respectively, according to the location of absorption bands. Parameterization of the single-scattering properties for ice cloud follows the procedure developed by Fu and Liou (1993). The spectral extinction coefficient, the single-scattering albedo, and the asymmetry factor are parameterized in terms of the IWC and the effective ice crystal size (D_e). For D_e, instead of using the mono-distribution as in the standard Fu-Liou code, we adopt the empirical formula for ice particle size distribution developed by McFarquhar and Heymsfield (1997, the MH distribution) as used in the MLS IWC forward model, where D_e is computed as a function of MLS measured IWC and temperature. This treatment of ice particle size is consistent with the MLS IWC retrieval and is better than other arbitrary assumption of ice particle size. We confine our attention to the effect of UTC at and above 215 hPa where MLS IWC measurements are valid. The radiative effect of all clouds throughout the tropospheric column can explored using CloudSat liquid and ice water contents in future work.

Because of the non-linearity of cloud radiation calculations, it is necessary to compute the radiative fluxes using instantaneous UTC profiles along orbit tracks, rather than using averaged profiles over a certain area or period. The monthly mean CRE is then constructed by averaging all individual CREs, totalling about 35000 calculations per month within the tropics (30°S-30°N). We consider that each measurement footprint has fractional cloud coverage η (whose determination is described later). Since the MLS measurement represents averaged IWC over the MLS FOV, the actual overcast IWC value is IWC/η. The total-sky radiative flux (F) for each MLS measurement area is thus

$$F = (1-\eta)F^{clr} + \eta F^{ov}, \qquad (1)$$

where F^{clr} and F^{ov} are clear-sky and overcast fluxes. The radiative effect of the MLS-observed cirrus is then defined as the difference between clear-sky and total-sky radiative fluxes at the top-of-atmosphere (TOA),

$$CRE = F^{clr} - F = \eta(F^{clr} - F^{ov}), \qquad (2)$$

with positive CRE indicating warming. We use the standard tropical atmosphere profile to compute F^{clr}. As elaborated in Soden et al. (2004), this method of cloud forcing calculation directly assesses the radiative perturbation due to clouds, and eliminates the impact of cloud-induced water vapor and temperature changes on radiative fluxes. However, direct comparison of such computed fluxes to observations is difficult as it is impossible to separate the effect of clouds and the effect of cloud-induced water vapor and temperature variations on observed radiative fluxes.

To obtain an estimate of the UTC fractional coverage η for each MLS IWC measurement, we interpolate the AIRS CFR onto the MLS IWC measurement location, assuming the MLS IWC in each UT layer overlaps in vertical. Sensitivity of CRE to the estimate of η is explored.

Insert Figure 4 here

Insert Figure 5 here

In the standard run, we assume that the emissivity of the observed UTC is 1 and thus the interpolated AIRS CFR on the MLS track equals the fractional coverage η. Figure 4 shows the maps of LW, SW and net CREs for January 2005 from the standard run. The model-computed CREs on orbit tracks have been averaged into 8° (in longitude) × 4° (in latitude) grid boxes. The corresponding maps of monthly mean MLS IWP and AIRS CFR (CTP < 300 hPa) for January 2005 are displayed in Fig. 5, with the same 8° × 4° horizontal gridding. The patterns of CREs resemble those of IWP and CFR. Large amplitudes of CREs are found over the climatological convective zones: the western Pacific, South America and South Africa, where high IWP and CFR are observed. The AIRS CFR indicates more cirrus than the MLS IWP in the regions away from deep convective centers, such as over the subtropics. The maximum LW warming amounts to 50 W m^{-2}, and is comparable to the maximum SW cooling. When averaged over the tropics from 30ºS to 30ºN, the mean LW CRE is 12.0 W m^{-2} and the mean SW CRE is –5.4 W m^{-2}, resulting in a net warming of 6.6 W m^{-2}. We compute the net cloud forcing for all months in 2005. The annual-mean tropical-mean UTC forcing is about 7.0 W m^{-2}.

To illustrate the dependence of the UTC radiative effect on IWP and CFR, we plot the LW, SW and net CRE distributions binned on MLS IWP and AIRS CFR for all individual measurements within 30°S-30°N in January 2005 (Fig. 6). The IWP bin intervals are specified logarithmically since a large number of samples are observed in the low IWP bins. The CFR bin interval is 15%. Within each IWP/CFR bin, the averaged CRE is shown.

Insert Figure 6 here

The visible optical depth of the UTC, obtained by averaging the model-derived visible optical depth for each IWP bin, is shown as a function of IWP by the grey line in Fig. 6b. The probability density functions (PDF) of MLS IWP and AIRS CFR are also shown in grey curves in Figs. 6c and 6f, respectively. The PDF of IWP exhibits a peak around 0.3 g m^{-2} and a broad distribution from a few g m^{-2} up to 100 g m^{-2}. About 95% of the observed IWP values are within 100 g m^{-2}. When IWP is greater than 100 g m^{-2}, the corresponding PDF decreases sharply. The visible optical depth derived from the Fu-Liou model for the observed UTC increases approximately linearly with IWP. The IWP of 100 g m^{-2} corresponds to $\tau = 2.5$. The maximum τ is about 3.5. Fewer than 1% of the individual IWP measurements have $\tau > 4$. Based on previous studies, high-altitude clouds with $\tau < 4$ have a dominant LW warming effect (Fu and Liou 1993; Choi et al. 2005; Choi and Ho 2006). Hence, it is not surprising that the LW warming effect outweighs the SW cooling effect for most of the observed UTC, resulting in a net warming over the entire tropics (Fig. 4c and Fig. 6c) The PDF of the CFR decreases monotonically with CFR, with a broad distribution between 20% and 80% (Fig. 6f grey curve).

The dependence of the CRE on IWP and CFR shown in Fig. 6 is consistent with the earlier radiative model calculations by Fu and Liou (1993), but our results assume the MH ice particle size distribution. The dependence of CRE on IWP is quite non-linear. When IWP is less than ~60 g m^{-2}, both LW and SW CRE magnitudes increase with IWP, with faster increase in LW CRE, resulting in increasing net warming effect. When IWP is between 60-100 g m^{-2}, the increase of

LW warming and SW cooling approximately cancel each other, producing very small change in the net CRE. When IWP is greater than 100 g m^{-2}, further increase of IWP favors SW cooling over LW warming, causing the net CRE to decrease sharply. Over the observed IWP range, the net CRE stays positive (warming). When CRE is binned on CFR (Fig. 6d-f), an approximately monotonic relation is found, with weak non-linearity existing for the SW CRE due to the rescaling of overcast IWP when CFR changes.

Two sets of sensitivity runs are conducted using the January 2005 cloud profiles. One set of experiments examine the uncertainty of CRE due to errors in the estimate of η. First, we add a correction factor of 0.2 to all CFR measurements following the preliminary analysis by Kahn et al. (personal communication, 2007) (the "+0.2 CFR run"). The resulting tropical-mean net CRE is 6.7 W m^{-2}, with the LW CRE being 10.9 W m^{-2} and the SW CRE being -4.2 W m^{-2} (Table 2). The increased cloud coverage estimate for each MLS FOV is associated with reduced overcast IWP due to the rescaling of IWP/η. The combined effects of increasing CFR and decreasing IWP contribute to a similar CRE as in the standard run. Second, we test an extreme case by assuming that the UTC coverage for each MLS IWC FOV is 100% and the AIRS CFR equals the cloud emissivity (the "overcast run"). In this case, the LW CRE increases substantially while the SW CRE decreases slightly, resulting in the net CRE of 16.7 W m^{-2}, about 10 W m^{-2} larger than the standard run (Table 2). Here, the effect due to increased cloud coverage is dominant in increasing the net cloud forcing.

Insert Figure 7 here

In the other set of sensitivity runs, we investigate the change of CRE due to changes of IWC by successively increasing IWC values at each level uniformly over the tropics by 25% to 250%, while keeping CFR unchanged. The results are shown in Fig. 7. The tropical-mean net warming reaches its maximum when IWC is increased by 50% from the current value. The net warming is 0.2 W m^{-2} more than the standard run, with LW and SW effects increasing by 1.9 and 1.7 W m^{-2}, respectively. Supposing the rate of IWC increase with SST is 20% K^{-1} as shown in Fig. 3a and Table 1, the change of net CRE is about 0.1 W m^{-1} K^{-1}, while the changes of LW and SW CRE are 1.0 and 0.9 W m^{-1} K^{-1}, respectively. When IWC is increased more than 50%, the increase in SW cooling outweighs LW warming, causing the net CRE reducing from its maximum value. When IWC is doubled, the net CRE returns to the approximately same value as the standard case, although the changes in the LW and SW effects are both as large as 3.2 W m^{-2} in the tropical average. Considering the low bias of 50% or so in the MLS IWC measurement (Wu et al. 2007), the doubled IWC run also gives the error in CRE due to the IWC retrieval. Further increase of IWC yields net warming smaller than the standard run, although it is unlikely the polarity of the net CRE would reverse sign given reasonable IWC changes for hypothetical SST changes within 5 K (corresponding to roughly doubled IWC change).

Note that the UTC forcing described above includes only the radiative effect of high-altitude clouds at 215 hPa and above. When clouds at lower altitudes are included, the net cloud forcing is different. It is expected that lower clouds would tend to have a stronger SW cooling effect that may overcome their LW warming effect.

5. Conclusion and discussion

Two aspects of tropical upper tropospheric cloud variations with SST are analyzed using AIRS, MLS and TRMM data. One aspect is UTC area fraction and the other is ice water content, which is directly linked to cloud optical thickness. Averages of cloud quantities are compared to those of SST and precipitation computed over “cloudy areas” defined with a consistent mask for each cloud quantity (see section 3) over the tropical oceans (30ºS-30ºN). Daily mean cloudy-area averaged UTC fraction (from AIRS) is nearly invariant with changes in the mean under-cloud SST (slightly increasing but with low correlation), while the tropical cloudy-area averaged precipitation increases with the mean under-cloud SST at a rate of ~20% K^{-1}. The UTC fraction increases with cloudy-area precipitation, but at a rate considerably slower than would be consistent with proportionality to precipitation. When we consider a normalization procedure that attempts to account for changes in intensity of convection by dividing by precipitation, the precipitation-normalized CFR thus yields a decreasing relationship to the mean under-cloud SST, dominated by the inverse of precipitation and SST relation. Measures of cloud ice, daily mean cloudy-area averaged IWC and IWP, are found to increase with the mean under-cloud SST, faster than does the corresponding cloudy-area averaged precipitation. Thus the precipitation-normalized IWP increases with the mean under-cloud SST.

Hence, the overall picture we obtain is that deep convection intensifies when local SST increases, which is associated with stronger rainfall and greater ice water content, but not greater coverage of upper tropospheric clouds. The UTC areal fraction tends to stay approximately constant when SST changes. The result that stronger convection produces thicker cirriform clouds when local SST increases is qualitatively consistent with RC1991, by examining the averaged UT IWC and IWP over the entire tropics (RC1991 focused on the Pacific with large El Niño signals). However, for the clouds analyzed in our study (215 hPa and above, possibly not as thick as those examined in RC1991), the cloud LW warming overcomes the SW cooling with no "thermostat" effect. Comparing the cloud fraction change with SST for the tropics-wide data sets used here to the Western Pacific infrared based results of LCH2001, we note a more complex relationship than the simplest version of the LCH2001 "iris" hypothesis. Using a precipitation-normalized CFR a decreasing tendency with SST similar to the cumulus-normalized anvil coverage in LCH2001 can be reproduced. However, while the intent of normalizing cloud statistics by a measure related to convective mass flux is appealing, a normalization procedure that assumes proportionality appears to face inherent problems. For the cloud fraction considered here, proportionality does not hold between CFR and precipitation. Furthermore, combining the linear fits of precipitation to mean under-cloud SST and cloud fraction to precipitation would yield different results than the directly estimated relationship of cloud fraction to SST which shows little relationship (a slight increase with low correlation). The correlations with SST, such as are examined here and in prior studies, do not exclude the effect of SST gradient and large-scale circulation, so extrapolation of the CFR and IWP relations with the mean under-cloud SST for cirrus change under global warming is subject to considerable caveats. Nonetheless, the observed variations of $\overline{CFR}^{c}$, $\overline{IWC}^{c}$, and $\overline{IWP}^{c}$ with the mean under-cloud SST provide useful measures of UTC variation with SST for evaluation of cloud simulations in climate models. Adequate representation of these relationships in present-day simulations is needed to obtain confidence that the models are able to accurately simulate future climate change.

Although the CFR appears to vary little with SST changes, the IWC and IWP have a robust increasing tendency with SST. We thus explore the radiative impact of IWC/IWP changes using the Fu-Liou radiative transfer model. We find that these upper-tropospheric clouds have a dominant infrared-warming effect, owing to their relatively small visible optical depth: 99% of the clouds have visible optical depth less than 4. The estimate of cloud fractional coverage has a substantial impact on the net UT cloud forcing, although the net forcing remains positive (warming) for all reasonable changes of CFR and IWP. The net cloud forcing increases by only about 0.2 W m^{-2} when IWC is increased by 50%, corresponding to a small positive feedback and a sensitivity to SST around 0.1 W m^{-2} K^{-1}. However, the small change in net CRE is associated with significant changes in LW and SW fluxes separately, which can have a non-negligible effect on atmospheric heating rate and surface energy budget. Further increase of IWC, by more than 50% would reduce the magnitude of net warming due to nonlinearity in the net CRE with IWC. When IWC is doubled, the net CRE is approximately the same as the current value.

Our estimate of net cloud forcing with IWC change assumes a uniform percentage increase of IWC over the tropics. It is not clear how the probability density function (including spatial distribution and occurrence frequency) of IWP would change during global warming. It is possible that varying IWC PDF would significantly change the net cloud forcing without changing the mean IWC given the non-linearity of cloud radiative forcing calculation. Therefore, it is also important to examine the change of IWC distributions (both spatially and temporally) with SST in addition to the mean IWC and SST relation. Continued monitoring and accurate measurements of these cloud properties are critical for climate modeling and climate change predictions.

Acknowledgments. We thank MLS and AIRS colleagues for data support. Discussions with A. Dessler, Q. Fu, B. Lin, R. S. Lindzen, and R. Rondanelli are helpful. This work was carried out at the Jet Propulsion Laboratory, California Institute of Technology, under contract with NASA.

References

Ackerman, S., K. Strabala, P. Menzel, R. Frey, C. Moeller, B. Gumley, B. Baum, S. W. Seeman, and H. Zhang, 2002: Discriminating clear-sky from cloud with MODIS-algorithm theoretical basis document (MOD35), in *MODIS Algorithm Theoretical Basis Document*, NASA.

Betts, A. K., Greenhouse warming and the tropical water budget, *Bull. Am. Meteorol. Soc. 71*, 1464-1465, 1990.

Bony, S., J.-L. Dufresne, H. LeTreut, J.-J. Morcrette, and C. Senior, 2004: On dynamic and thermodynamic components of cloud changes. *Climate Dyn*., **22**, 71-86.

Cess R. D., Coauthors, 1990: Intercomparison and interpretation of climate feedback processes in 19 atmospheric GCMs. *J. Geophys. Res.*, **95**, 16601–16615.

Cess R. D., Coauthors, 1996: Cloud feedback in atmospheric general circulation models: An update. *J. Geophys. Res.*, **101**, 12791–12794.

Chahine M. T, T. S. Pagano, H. H. Aumann, R. Atlas, C. Barnet, et al. (2006) AIRS: Improving Weather Forecasting and Providing New Data on Greenhouse Gases. *Bull. Am. Meteorol. Soc.*: Vol. 87, No. 7 pp. 911–926.

Chambers L., B. Lin, and D. Young, 2002: New CERES data examined for evidence of tropical iris feedback. *J. Clim.*, **15**, 3719–3726.

Choi, Y.-S., C.-H. Ho, C.-H. Sui, 2005: Different optical properties of high cloud in GMS and MODIS observations, *Geophys. Res. Lett.,* 32, L23823, doi:10.1029/2005GL024616.

Choi, Y.-S., and C.-H. Ho, 2006: Radiative effect of cirrus with different optical properties over the tropics in MODIS and CERES observations, Geophys. Res. Lett., 33, L21811, doi:10.1029/2006GL027403.

Chou, C. and J. D. Neelin, 1999: Cirrus detrainment-temperature feedback. *Geophys. Res. Lett.,* **26**(9), 1295-1298.

Chou, M.-D., R. S. Lindzen, and A.Y. Hou, 2002: Reply to: "Tropical cirrus and water vapor: an effective Earth infrared iris feedback?" *Atmospheric Chemistry and Physics*, **2**, 99-101.

Chou, M.-D., R. S. Lindzen, and A.Y. Hou, 2002b: Comments on "The Iris hypothesis: A negative or positive cloud feedback?" *J. Climate*, **15**, 2713-2715.

Del Genio A. D., and W. Kovari. 2002: Climatic properties of tropical precipitating convection under varying environmental conditions. *J. Clim*. 15, 2597-2615.

Donlon, C. J., P. Minnett, C. Gentemann, T. J. Nightingale, I. J. Barton, B. Ward and, J. Murray, 2002: Towards Improved Validation of Satellite Sea Surface Skin Temperature Measurements for Climate Research, *J. Clim,* **15**, No. 4, 353-369.

Fu, R., A. D. Del Genio, W. B. Rossow, and W. T. Liu, Cirrus-cloud thermostat for tropical sea surface temperatures tested using satellite data, *Nature*, 358, 394-397, 1992.

Fu, Q., and K.N. Liou, 1992: On the correlated k-distribution method for radiative transfer in nonhomogeneous atmospheres. *J. Atmos. Sci.*, 49, 2139-2156.

Fu, Q., and K. N. Liou, 1993: Parameterization of the radiative properties of cirrus clouds. *J. Atmos. Sci.,* 50, 2008-2025.

Fu, Q., K.N. Liou, M. Cribb, T.P. Charlock, and A. Grossman, 1997: Multiple scattering in thermal infrared radiative transfer. *J. Atmos. Sci.*, 54, 2799-2812.

Fu, Q., M. Baker, D. L. Hartmann, 2002: Tropical cirrus and water vapor: An effective earth infrared iris feedback? *Atmos. Chem. Phys.*, 2, 1-7.

Gao, B. C., P. Yang, W. Han, R. R. Li, and W. J. Wiscombe, 2002: An algorithm using visible and 1.38 μm channels to retrieve cirrus reflectances from aircraft and satellite data, *IEEE Trans. Geosci. Remote Sens.*, *40*, 1659–1668.

Graham, N. E. and T. P. Barnett, Sea surface temperature, surface wind divergence, and convection over tropical oceans. *Science, 238,* 657-659,1987.

Hartmann, D.L., and M.L. Michelsen, 1993: Large-scale effects on regulation of tropical sea surface temperature. *J. Clim., 6,* 2049-2062.

Hartmann, D. L. and K. Larson, 2002: An Important Constraint on Tropical Cloud-Climate Feedback. *Geophys. Res. Lett.*, *29*(20), 1951-1954.

Hartmann D. L., and M. L. Michelsen, 2002: No evidence for iris. *Bull. Amer. Meteor. Soc.*, 83, 249-254.

Huffman, G. J., R.F. Adler, M. Morrissey, D.T. Bolvin, S. Curtis, R. Joyce, B McGavock, J. Susskind, 2001: Global Precipitation at One-Degree Daily Resolution from Multi-Satellite Observations. J. Hydrometeor., 2(1), 36-50.

Kahn, B.H., A. Eldering, A.J. Braverman, E.J. Fetzer, J.H. Jiang, E. Fishbein, and D.L. Wu, 2007: Towards the characterization of upper tropospheric clouds using Atmospheric Infrared Sounder and Microwave Limb Sounder observations, *J. Geophys. Res. 112*, D05202, doi:10.1029/2006JD007336.

Lau, K.-M., H.-T. Wu, S. Bony, 1997: The role of large-scale atmospheric circulation in the relationship between tropical convection and sea surface temperature, *J. Clim*, **10**, 381-392

Li, J.-L., D.E. Waliser, J.H. Jiang, D.L. Wu, W.G. Read, J.W. Waters, A.M. Tompkins, L.J. Donner, J.-D. Chern, W.-K. Tao, R. Atlas, Y. Gu, K.N. Liou, A. Del Genio, M. Khairoutdinov, and A. Gettelman, 2005: Comparisons of EOS MLS Cloud Ice Measurements with ECMWF analyses and GCM Simulations: Initial Results, *Geophys. Res. Lett*. 32 , L18710, doi:10.1029/2005GL023788.

Lin B., B. Wielicki, L. Chambers, Y. Hu, and K.-M. Xu, 2002: The iris hypothesis: A negative or positive cloud feedback? *J. Climate*, **15**, 3-7.

Lin, B., B. A. Wielicki, P. Minnis, L. Chambers, K.-M. Xu, Y. Hu, and A. Fan, 2006: The effect of environmental conditions on tropical convective systems observed from the TRMM satellite, *J. Clim*, **19**, 5745-5761.

Lindzen, R. S., 1990: Some coolness concerning global warming. *Bull. Amer. Meteor. Soc*. **71**, 288-299.

Lindzen, R. S., and S. Nigam, 1987: On the role of sea surface temperature gradients in forcing low level winds and convergence in the tropics. *J. Atmos. Sci*., **44**, 2418-2436.

Lindzen, R. S., M.-D. Chou, and A. Y. Hou, 2001: Does the Earth have an adaptive infrared iris, *Bull. Am. Meteorol. Soc,* 82, 417-432.

Lindzen, R. S., M.-D. Chou, and A.Y. Hou, 2002: Comments on "No evidence for iris." *Bull. Amer. Met. Soc.*, **83**, 1345-1348.

Liou, K.N., Q. Fu, and T.P. Ackerman, 1988: A simple formulation of the delta-four-stream approximation for radiative transfer parameterizations. *J. Atmos. Sci.*, 45, 1940-1947.

Liou, K.-N., 2002: An Introduction to Atmospheric Radiation (second edition), Academic Press, New York, 583 pp.

Liu, X., J. E. Penner, S. J. Ghan and M. Wang, 2007: Inclusion of ice microphysics in the NCAR community atmospheric model version 3 (CAM3), *J. Clim*., submitted.

Livesey, N. J., et al., EOS MLS Version V1.5 Level 2 data quality and description document, 2005, available at http://mls.jpl.nasa.gov.

Massie, S., A. Gettelman, W. Randel, and D. Baumgardner, 2002: Distribution of tropical cirrus in relation to convection, *J. Geophys. Res.*, *107*, doi:10.1029/2001JD001293, 2002.

McFarquhar, G. M., and A. J. Heymsfield, 1997: Parameterization of tropical cirrus ice crystal size distributions and implications radiative transfer: Results from CEPEX. *J. Atmos. Sci.,* 54, 2187-2200.

Olsen, E. T., ed., AIRS/AMSU/HSB Version 4.0 Data Release User Guide, JPL Document, 2005.

Parkinson, C. L., 2003: Aqua: An Earth-observing satellite mission to examine water and other climate variables, *IEEE Trans. Geosci. Remote Sens.*, 41 (2), 173-183.

Pierrehumbert, R. T., Thermostats, radiator fins, and the local runaway greenhouse, *J. Atmos. Sci*., *52*, 1784-1806, 1995.

Ramanathan, V., and W. Collins, 1991: Thermodynamics regulation of ocean warming by cirrus clouds deduced from observations of the 1987 El Nino, *Nature*, **351**, 27-32.

Ramanathan V., R. D. Cess, E. F. Harrison, P. Minnis, B. R. Barkstrom, E. Ahmad, and D. Hartmann, 1989: Cloud radiative-forcing and climate: Results from the Earth Radiation Budget Experiment. Science, 243, 57-63.

Raval, A., and V. Ramanathan, Observational determination of the greenhouse effect, *Nature, 342,* 758-762, 1989.

Schoeberl, et al., Overview of the EOS Aura Mission, 2006: *IEEE Trans. Geosci. Remote Sensing,* **44**, 1066-1074.

Schoeberl, M. R. and S. Talabac, "The Sensor Web: A future Technique for Science Return, in Observing Systems for Atmospheric Composition, 2006, G. Visconti, P. DiCarlo, B. Brune, M. Schoeberl, A. Wahner, Eds, Springer, NY, pgs. 203-206.

Soden, B. J., and R. Fu, 1995: A Satellite Analysis of Deep Convection, Upper-Tropospheric Humidity, and the Greenhouse Effect, *J. Clim*, *8*, 2333-2351.

Soden, B. J, Broccoli A. J., and Hemler R. S., 2004: On the Use of Cloud Forcing to Estimate Cloud Feedback. *J. Clim*, 17, 3661–3665.

Stephens, G. L., D. G. Vane, R. Boain, G. Mace, K. Sassen, Z. Wang, A. Illingworth, E. O'Connor, W. Rossow, S. L. Durden, S. Miller, R. Austin, A. Benedetti, C. Mitrescu, and the CloudSat Science Team, 2002: The CloudSat Mission and the A-Train: A new dimension of space-based observations of clouds and precipitation. *Bull. Amer. Meteor. Soc.*, **83** (12), 1771-1790.

Stephens, G. L. 2005: Cloud feedbacks in the climate system: A critical review. *J. Climate*, **18**, 237–273.

Su, H., W. G. Read, J. H. Jiang, J. W. Waters, D. L. Wu, and E. J. Fetzer, 2006: Enhanced positive water vapor feedback associated with tropical deep convection: New evidence from Aura MLS, *Geophys. Res. Lett.* 33, L05709, doi:10.1029/2005GL025505.

Sun, D. Z., and R. S. Lindzen, 1993: Distribution of tropical tropospheric water vapor, *J. Atmos. Sci*., *50*, 1644-1660.

Sun, D. Z. and Z. Liu, Dynamic ocean-atmosphere coupling: a thermostat for the tropics. *Science*, 272, 1148-1150, 1996.

Susskind, J., C. D. Barnet, and J. M. Blaisdell, 2003: Retrieval of atmospheric and surface parameters from AIRS/AMSU/HSB data in the presence of clouds, *IEEE Trans. Geosci. Remote Sens.,* 41, 390-409.

Tompkins A. M., and Craig G. C., 1999: Sensitivity of Tropical Convection to Sea Surface Temperature in the Absence of Large-Scale Flow. Journal of Climate: Vol. 12, No. 2 pp. 462–476.

Udelhofen, P. M., and D. L. Hartmann, D. L., 1995: Influence of tropical cloud systems on the relative humidity in the upper troposphere, *J. Geophys. Res.*, *100*, 7423-7440.

Waliser, D. E, N. E.Graham, and C. Gautier, 1993: Comparison of the Highly Reflective Cloud and Outgoing Longwave Radiation Datasets for Use in Estimating Tropical Deep Convection. *J. Clim.,* 6, 331–353.

Wallace, J. M., Effect of deep convection on the regulation of tropical sea surface temperature, Nature, 357, 230-231, 1992.

Waters, J. W., et al., 2006: The Earth Observing System Microwave Limb Sounder (EOS MLS) on the Aura satellite, *IEEE Trans. Geosci. Remote Sensing,* **44**, 1075-1092.

Wu, D. L., J. H. Jiang, and C. P. Davis, 2006: EOS MLS cloud ice measurements and cloudy-sky radiative transfer model, *IEEE Trans. Geosci. Remote Sensing,* **44**, 1156-1165.

Wu, D. L., J. H. Jiang, William G. Read, et al, 2007: Validation of Aura MLS cloud ice water content measurements, *J. Geophys. Res.*, submitted.

Table Captions

Table 1. Regression slopes (in the units of percentage change K^{-1}, relative to the long-term means) of AIRS cirrus fraction (CTP < 300 hPa) and MLS IWP (from 215 hPa and up) versus the mean under-cloud SST for different tropical bands.

	CFR	Precipitation-normalized CFR	IWP	Precipitation-normalized IWP
30ºS-30ºN	2%	–24%	19%	8%
20ºS-20ºN	4%	–21%	22%	14%
10ºS-10ºN	8%	–23%	31%	19%
30ºS-30ºN, 130ºE-170ºW (as in LCH)	6%	–12%	19%	6%

Table 2. Tropical-mean (30°S-30°N) LW, SW and net CRE (in W m^{-2}) in January 2005 for the radiative model runs with different cloud fraction coverage estimates.

	LW CRE	SW CRE	Net CRE
Standard run	12.0	–5.4	6.6
+0.2 CFR run	10.9	–4.2	6.7
Overcast run	20.3	–3.6	16.7

Figure Captions

Figure 1. Scatter plots of (a) the tropical-averaged (30ºS-30ºN) CFR (CTP < 300 hPa) versus mean under-cloud SST; (b) the tropical-averaged CFR versus the tropical cloudy-area (CFR > 0) averaged precipitation; (c) the tropical cloudy-area averaged precipitation versus the mean under-cloud SST; and (d) the precipitation-normalized CFR (in % mm^{-1} day) versus the mean under-cloud SST. Each point is a daily value from September 1, 2002 to September 30, 2006. The solid lines are the least squares linear fits to the data, with the corresponding equations shown. The dotted line in Fig. 1b marks the regression line constrained to go through zero (see text for details).

Figure 2. Scatter plots of tropical-averaged (30ºS-30ºN) IWC versus the mean under-cloud SST at three pressure levels, (a) 100 hPa, (b) 147 hPa and (c) 215 hPa; and (d) the MLS-derived CTP versus the mean under-cloud SST. Each point is a daily value from August 8, 2004 to September 30, 2006. The solid lines are the least squares linear fits to the data, with the corresponding equations shown.

Figure 3. Scatter plots of (a) the tropical-averaged (30ºS-30ºN) IWP (integrated from 215 hPa) versus the mean under-cloud SST; (b) the tropical-averaged IWP versus the tropical cloudy-area (IWP > 0) averaged precipitation; (c) the tropical cloudy-area averaged precipitation versus the mean under-cloud SST; and (d) the precipitation-normalized IWP (in g m^{-2} mm^{-1} day) versus the mean under-cloud SST. Each point is a daily value from August 8, 2004 to September 30, 2006. The solid lines are the least squares linear fits to the data, with the corresponding equations shown. The dotted line in Fig. 3b marks the regression line constrained to go through zero (see text for details).

Figure 4. Horizontal maps of model-computed CREs at the top-of-atmosphere for the MLS-observed cirrus clouds (215 hPa and up) for January 2005, (a) LW, (b) SW and (c) net CRE, with positive sign indicating warming to the Earth-atmosphere and vice versa.

Figure 5. Horizontal maps of the monthly mean MLS IWP and AIRS CFR for January 2005.

Figure 6. The model-computed LW, SW and net CRE binned on MLS IWP (a-c) and AIRS CFR (d-f) (black lines) for January 2005. The grey line in (b) is the model-computed mean visible optical depth for

each IWP bin. The grey lines in (c) and (f) are the probability density function of MLS IWP and AIRS CFR for January 2005, respectively. The horizontal dotted lines in (c) and (f) mark the zero net CRE.

Figure 7. The difference of tropical-mean (a) net, (b) LW and SW CRE (in W m^{-2}) between the runs with increased IWP and the standard run. All results are based on the January 2005 cloud profiles.

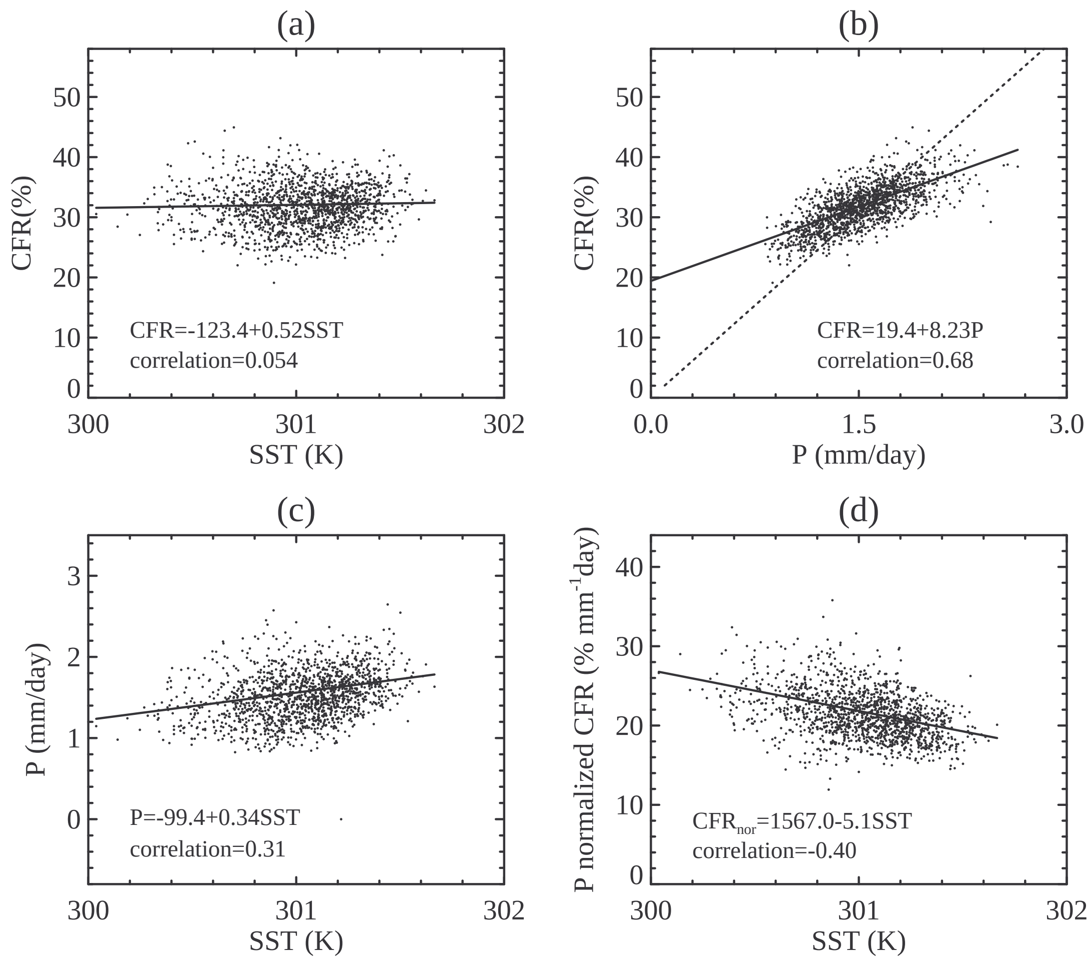

Figure 1. Scatter plots of (a) the tropical-averaged (30ºS-30ºN) CFR (CTP < 300 hPa) versus the mean under-cloud SST; (b) the tropical-averaged CFR versus the tropical cloudy-area (CFR > 0) averaged precipitation; (c) the tropical cloudy-area averaged precipitation versus the mean under-cloud SST; and (d) the precipitation-normalized CFR (in % mm^{-1} day) versus the mean under-cloud SST. Each point is a daily value from September 1, 2002 to September 30, 2006. The solid lines are the least squares linear fits to the data, with the corresponding equations shown. The dotted line in Fig. 1b marks the regression line constrained to go through zero (see text for details).

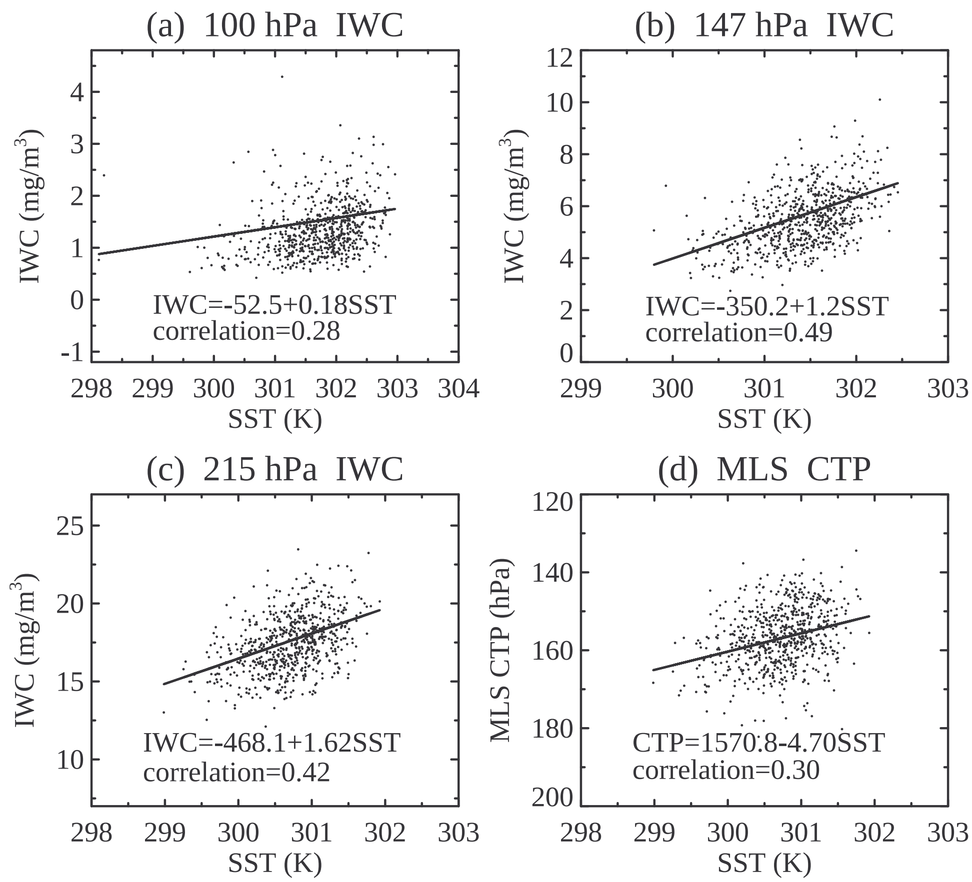

Figure 2. Scatter plots of tropical-averaged (30ºS-30ºN) IWC versus the mean under-cloud SST at three pressure levels, (a) 100 hPa, (b) 147 hPa and (c) 215 hPa; and (d) the MLS-derived CTP versus the mean under-cloud SST. Each point is a daily value from August 8, 2004 to September 30, 2006. The solid lines are the least squares linear fits to the data.

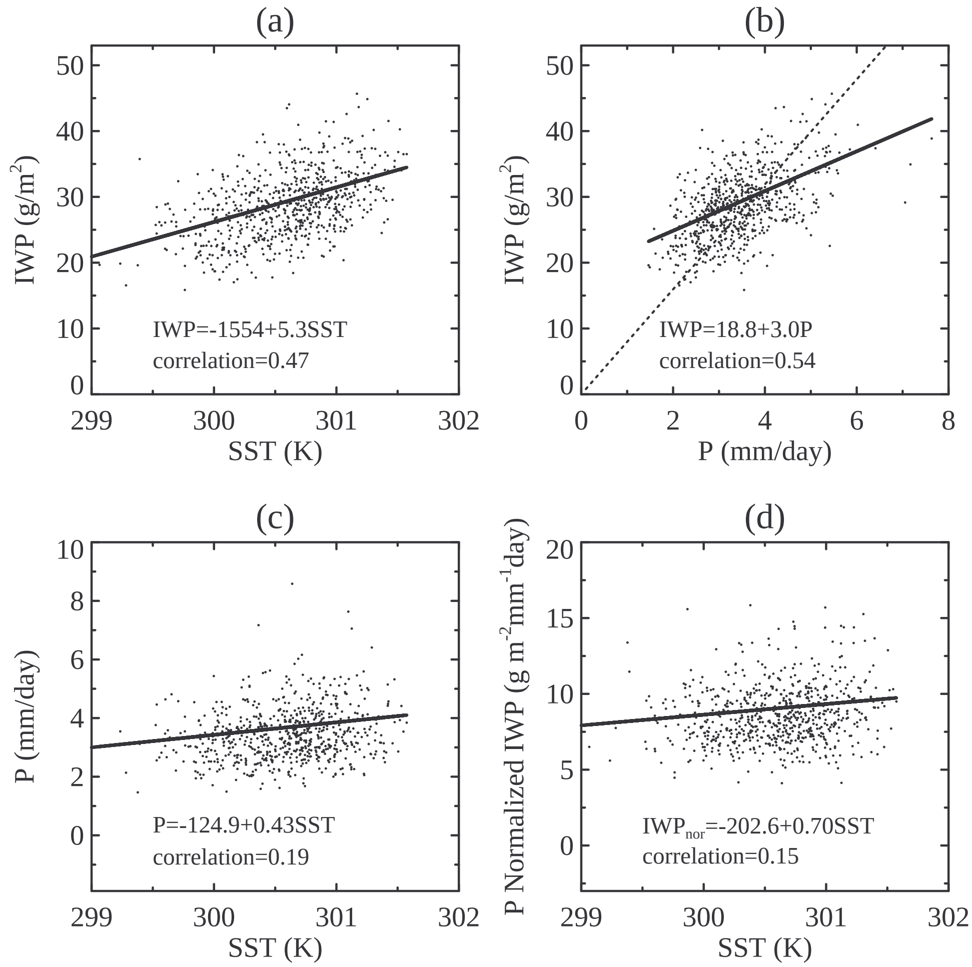

Figure 3. Scatter plots of (a) the tropical-averaged (30ºS-30ºN) IWP (integrated from 215 hPa) versus the mean under-cloud SST; (b) the tropical-averaged IWP versus the tropical cloudy-area (IWP > 0) averaged precipitation; (c) the tropical cloudy-area averaged precipitation versus the mean under-cloud SST; and (d) the precipitation-normalized IWP (in g m^{-2} mm^{-1} day) versus the mean under-cloud SST. Each point is a daily value from August 8, 2004 to September 30, 2006. The solid lines are the least squares linear fits to the data, with the corresponding equations shown. The dotted line in Fig. 1b marks the regression line constrained to go through zero (see text for details).

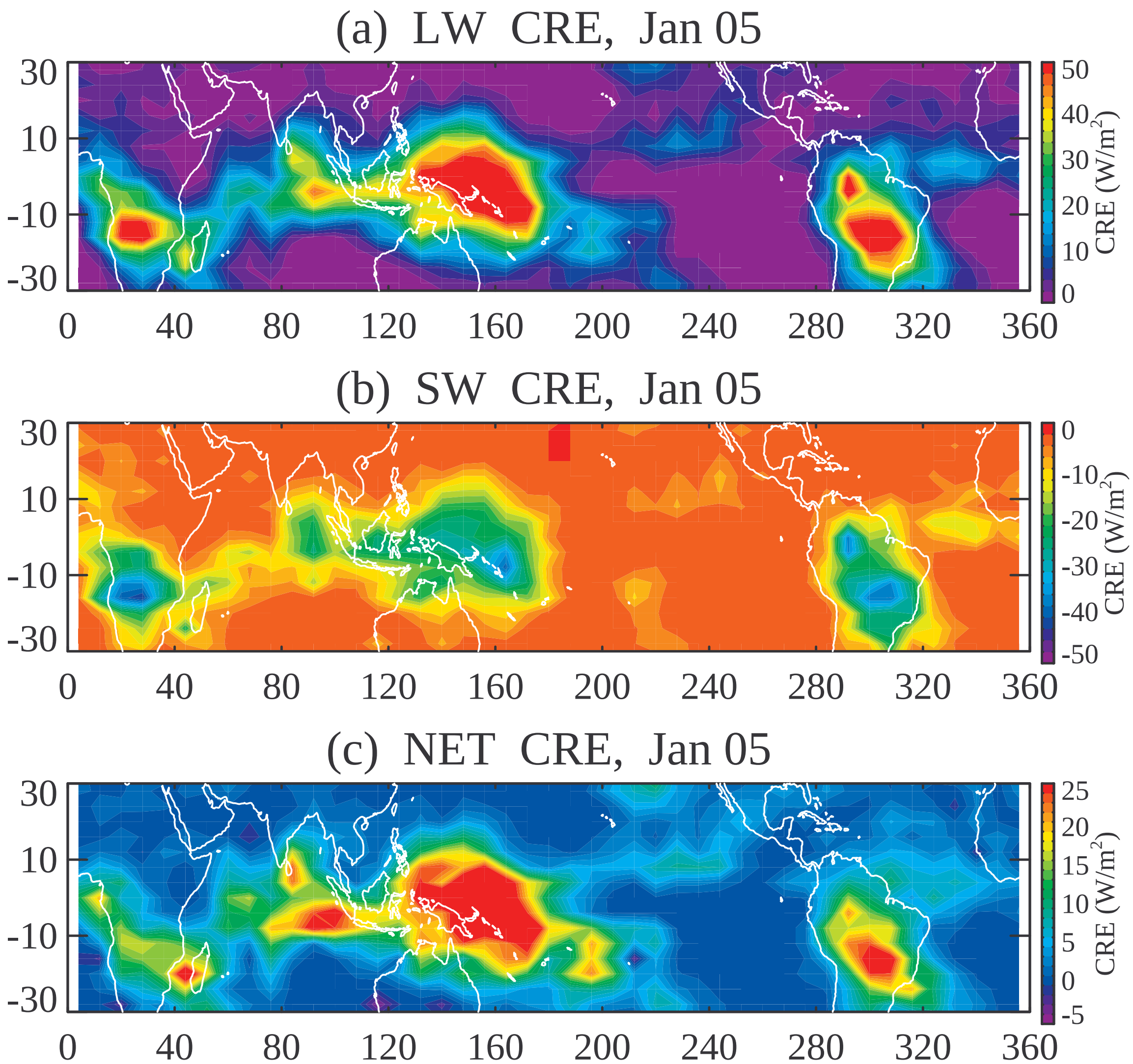

Figure 4. Horizontal maps of model-computed CREs at the top-of-atmosphere for the MLS-observed cirrus clouds (215 hPa and up) for January 2005, (a) LW, (b) SW and (c) net CRE, with positive sign indicating warming to the Earth-atmosphere and vice versa.

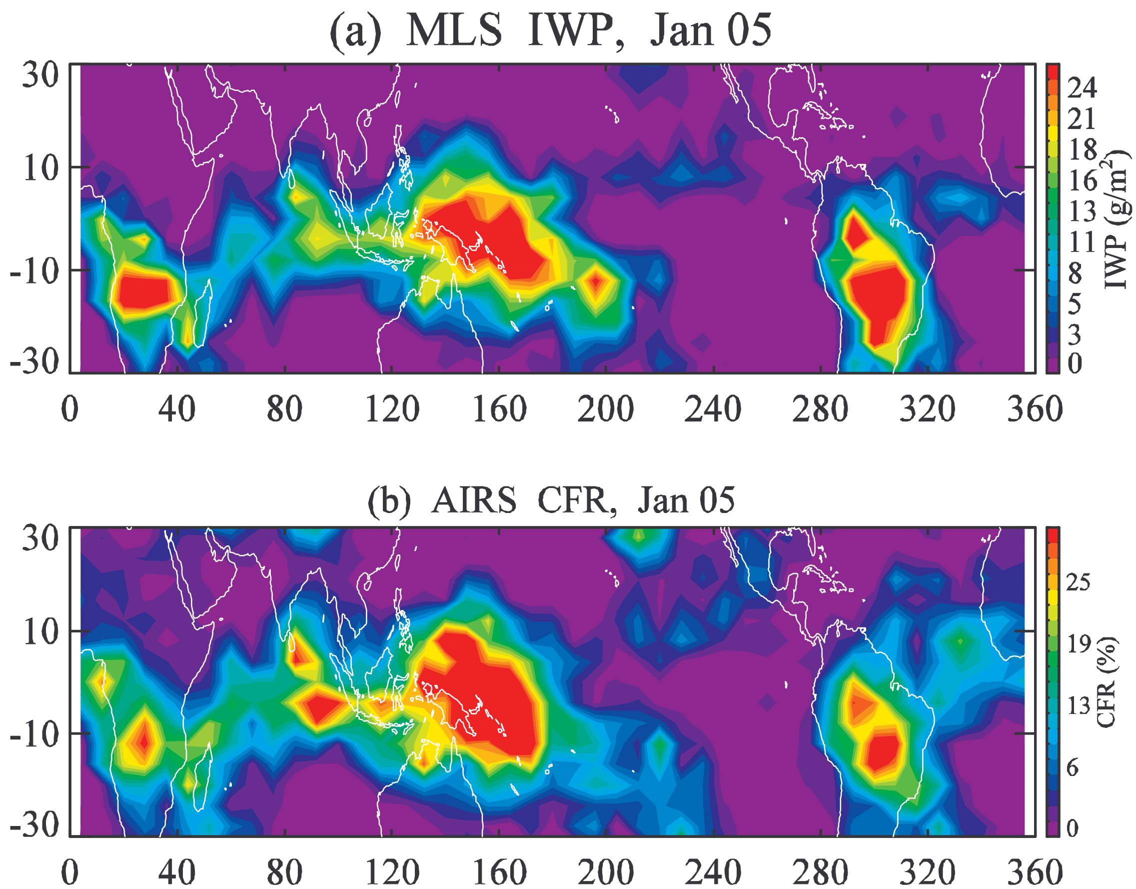

Figure 5. Horizontal maps of the monthly mean MLS IWP and AIRS CFR for January 2005.

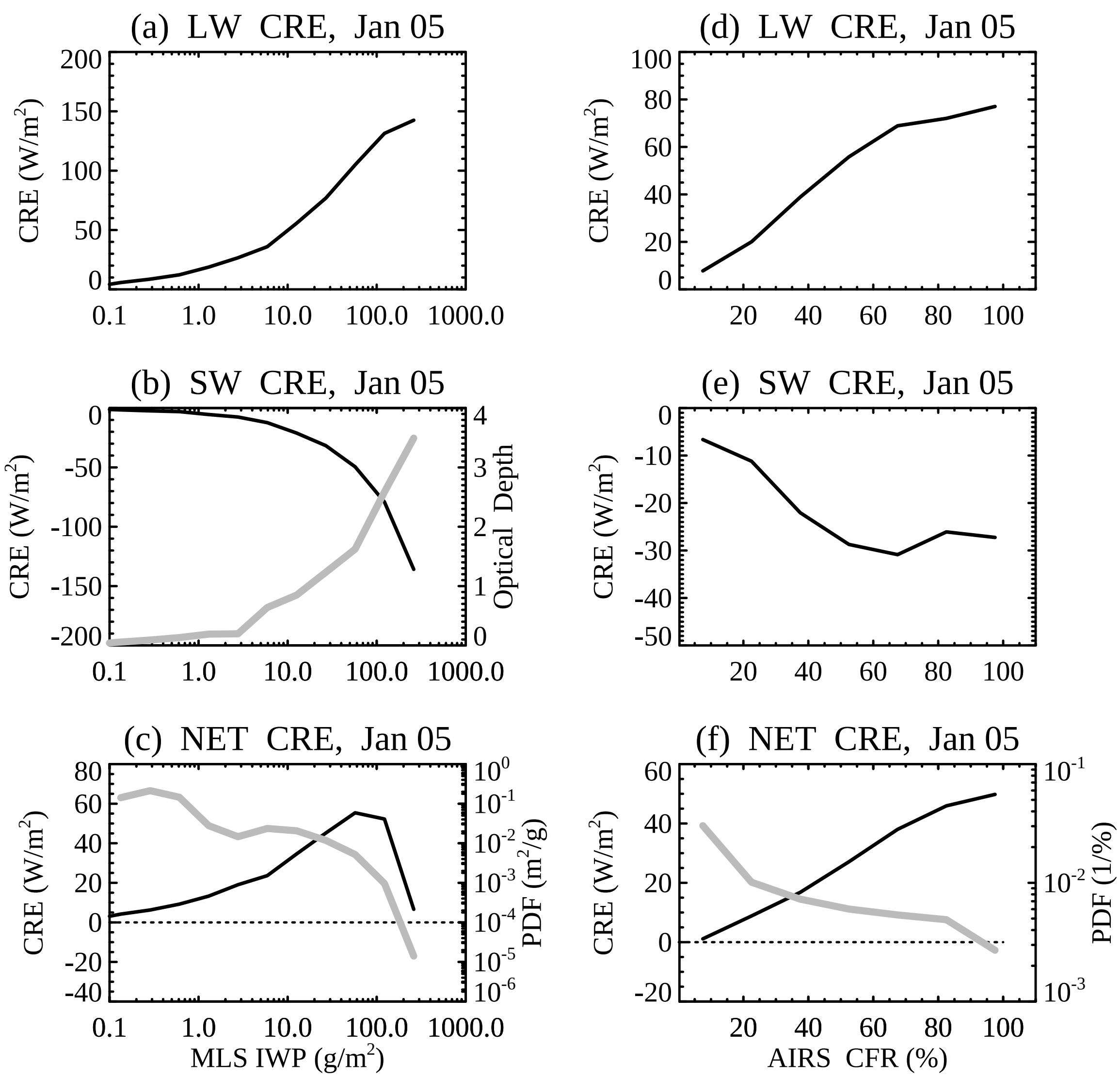

Figure 6. The model-computed LW, SW and net CRE binned on MLS IWP (a-c) and AIRS CFR (d-f) (black lines) for January 2005. The grey line in (b) is the model-computed mean visible optical depth for each IWP bin. The grey lines in (c) and (f) are the probability density function of MLS IWP and AIRS CFR for January 2005, respectively. The horizontal dotted lines in (c) and (f) mark the zero net CRE.

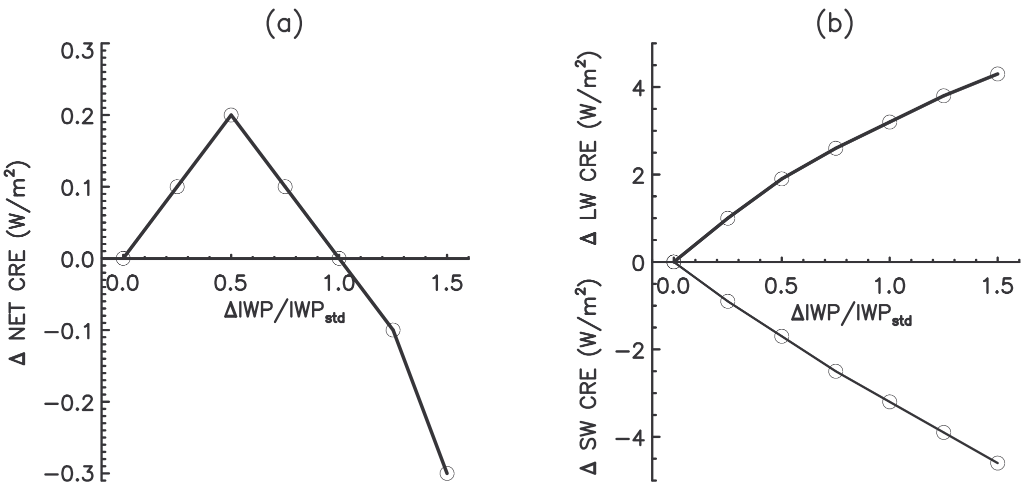

Figure 7**.** The difference of tropical-mean (a) net, (b) LW and SW CRE (in W m^{-2}) between the runs with increased IWP and the standard run. All results are based on the January 2005 cloud profiles.